REPORT DOCUMENTATION PAGE 1 0 MAR 1998

Form Approved
OMB No. 0704-0188

1. AGENCY USE ONLY (Leave blank)	2. REPORT DATE	3. REPORT TYPE AND DATES COVERED
	31 January 1998	Final Technical Report: 1/5/ 94 - 31/10/1997

4. TITLE AND SUBTITLE

(HBCU) Thermal-Electric Propulsion with Magnetoplasmadynamic Acceleration

5. FUNDING NUMBERS

G - F49620-94-1-0263

6. AUTHOR(S)

Bagher M. Tabibi, Dung X. Nguyen, and Ja H. Lee

7. PERFORMING ORGANIZATION NAMES(S) AND ADDRESS(ES)

Hampton University
Queen Street
Hampton, VA 23668

AFRL-SR-BL-TR-98-

0293

APL - 97

9. SPONSORING / MONITORING AGENCY NAMES(S) AND ADDRESS(ES)   N/A

AFOSR/NA
110 Duncan Avenue, Suite B115
Bolling AFB, DC 20332 - 0001

10. SPONSORING / MONITORING AGENCY REPORT NUMBER

11. SUPPLEMENTARY NOTES

a. DISTRIBUTION / AVAILABILITY STATEMENT

Approved for public release; distribution is unlimited

12. DISTRIBUTION CODE

19980414 136

13. ABSTRACT (Maximum 200 words)

A solar thermal-electric propulsion (STEP) system has been installed to develop a rocket engine having medium ranges of specific impulse and thrust. The STEP system consisted of a solar thermal and a magnetoplasmadynamic (MPD) thrusters in a tandem arrangement. The thermal chamber temperature versus the optical power was evaluated to be adequate. Without the DC power on the MPD electrodes, the system merely produce a thermal plume of argon gas. An insitu technique, Pitot tube method, was used to measure the total and static pressures of the core flow of the thermal plume in steady-state operation in order to characterize and benchmark so that any increment of thrust and specific impulse resulted from the MPD acceleration. The data were compared with the results of CET'93 computer code developed at NASA Lewis Research Center. An increase in the total pressure, therefore the thrust, was found to be proportional to the square of MPD current as expected. The relative increase in total pressure was approximately 40% when the MPD current reached to 500 A.

DTIC QUALITY INSPECTED 4

14. SUBJECT TERMS	15. NUMBER OF PAGES
Advanced propulsion system, solar thermal propulsion, MPD thruster, upperstage propulsion.	21
	16. PRICE CODE

17. SECURITY CLASSIFICATION OF REPORT	18. SECURITY CLASSIFICATION OF THIS PAGE	19. SECURITY CLASSIFICATION OF ABSTRACT	20. LIMITATION OF ABSTRACT
UNCLASSIFIED	UNCLASSIFIED	UNCLASSIFIED	UL

Standard Form 298 (Rev. 2-89)
Prescribed by ANSI Std Z39-18
298-102

CONTENTS

2. TECHNICAL BRIEF

2.1.1 Introduction

In recent years many efforts have been rendered to develop more practical orbit transfer vehicles (OTV) between LEO and GEO. Birkan et al. [1] discussed on laser and electric propulsion devices for OTV missions in terms of specific impulse, thrust density and power processor efficiency against the specific mass. According to this analysis, magnetoplasmadynamic (MPD) thrusters when powered by solar energy, like most of other electric propulsion devices, were estimated to have the initial mass lower than a typical chemical rocket, but its trip time was more than 100 times that of chemical rocket because of its low thrust. An MPD thruster may have the payload fraction of 0.7 - 0.9 close to that of ion thrusters, much higher than that (about 0.2) of a chemical rocket, and produce a middle range of thrust density compared with those of ion and chemical thrusters [2], so that it might offer itself an effective, low cost thruster if its thrust is further improved. Many experiments have been conducted with MPD thrusters in pulsed modes [3,4], as well as in steady state modes [5,6] to increase the thrust. MPD thruster could generate specific impulse up to 11000 sec [7], but its thrust is much lower than the thrust of chemical and or thermal thrusters. The specific impulse of the thermal thrusters is limited to 1000 sec because there is no proper material contain the propellant gas having the temperature over 4000 K [8] while its thrust reaches up to 91383 N [9]. For practical space application, both thrust and specific impulse are equally important.

We presented earlier a new concept called solar thermal-electric propulsion (STEP)[10] that combines a solar thermal and a solar electric thrusters in tandem arrangement to enhance the thrust and specific impulse in a single system. According to our estimations, the STEP system may attain the specific impulse up to 3,567 sec at a thrust of 341 N with a throat of 30-mm diameter [10,11]. From these studies, a STEP system has been designed and installed to prove its concept [12] (see Figure 1). This report summarizes the significant work accomplished during the three and half year period of funding from 1993 to 1997.

This final technical report summarizes the project effort in Experimental Setup which includes Propellant Supply unit, Solar Simulator and Collector mirror, the MPD thruster, Test Section and Diagnostic instruments, and the experimental results with data analysis.

Publications and graduate students training are also summarized.

2.1.2 Experimental Setup

As seen in the Figure 1, the STEP system is consisted of gas supplies, a thermal thruster which is heated by a solar simulator arc-lamp, an elliptical collector mirror, an

3

MPD thruster with power supplies, a two-section stainless steel test chamber with three windows in first section and four windows in second section, a 30-m^3 capacity vacuum tank with two gate valves located at both ends, a 3-stage vacuum pumping system, two cooling units, an excimer-pumped dye laser, and measurement instruments. The fundamental parts of the experimental setup and their functioning are detailed in the following
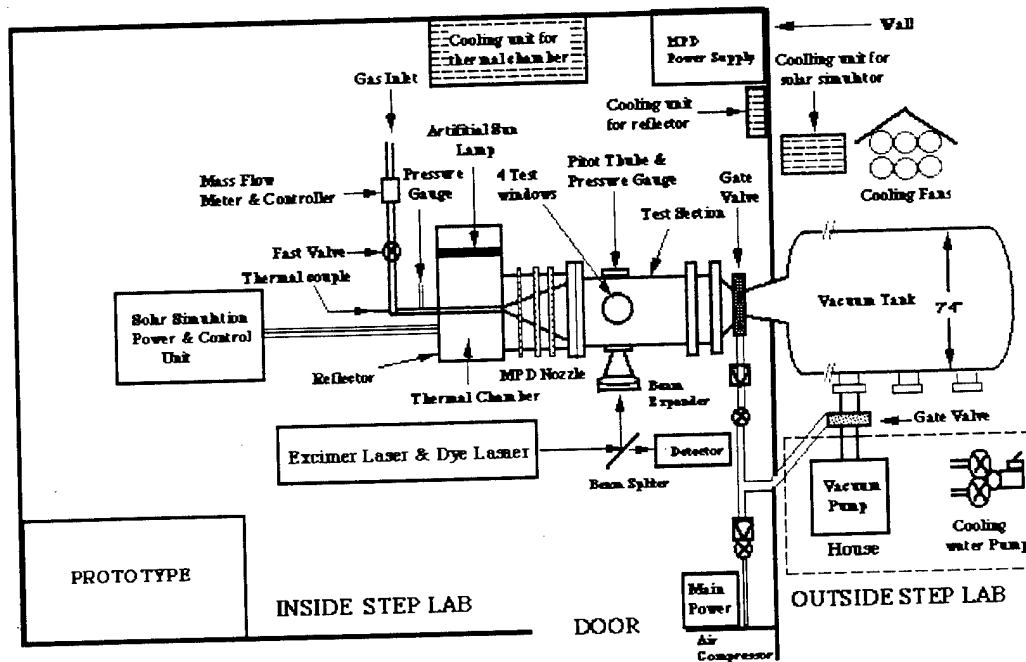

Figure 1. Schematic of Solar Thermal-Electric Propulsion System.

2.1.3 Thermal Thruster and Propellant Supply

The thermal thruster, shown in Figure 2, is an integrated unit of a thermal chamber and a converging-diverging nozzle. The stainless-steel thermal chamber is placed along a focal line of the elliptical reflector mirror which focuses the light emitted from the solar simulator arc-lamp placed along the conjugate focal line. The thermal chamber surrounded by two quartz tubes (inner one and outer one). The inner quartz tube of the dimension of 35x38x237 mm is used to keep vacuum, obtained by a separate vacuum pump, around the thermal chamber to keep it from oxidization at high temperatures. The outer quartz tube of dimension of 47x50x203 mm kept the cold water, provided by a refrigerated cooling unit (Electra Impulse, Inc., RU-400 series: flow rate = 1.5x10^{-2} m^3/s), to circulate through the space between it and the inner tube. The cold water could also be circulated through the two end holders of the tubes and thermal chamber.

(Unit : mm)
(Not Scaled)

2.5 thickness

7.5 °   30 °

19.05

44.0

31.6
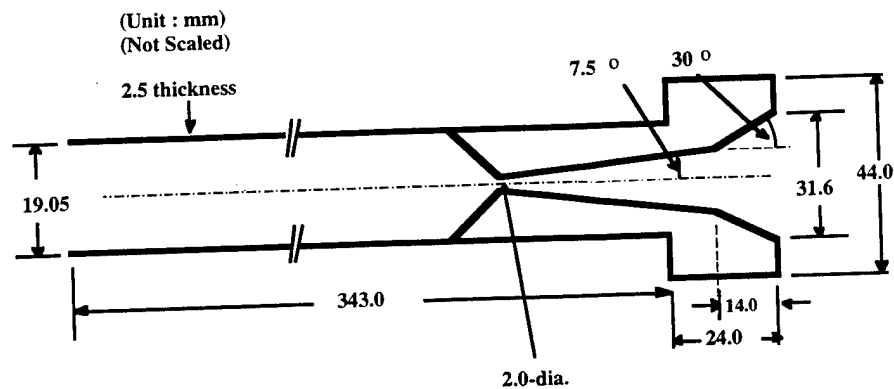
343.0

14.0

24.0

2.0-dia.

Figure 2. Configuration of the stainless-steel thermal chamber and nozzle

The propellant gas stored in a gas cylinder entered into the thermal chamber through a fast acting valve (Swagelock Co., SS-63TS8-330D). The thermal chamber heated by the solar simulator arc-lamp, heats in turn the propellant passing through it by mainly convective heat transfer. A K-type thermocouple (Omega Engineering Inc., EI1101515/TJ120-CASS-116E-23/1/8") measured the temperature of the gas inside the stainless steel thermal chamber. However, a C-type thermocouple (Omega Engineering Inc., XMO-W5R26-U-125-30-B-1-08: Exotic probe, Molybdenum) with a maximum operating temperature of 2500 K was used when a tungsten thermal chamber replaced the stainless steel one. A pressure transducer (MKS Instrument Co., Model 122-AA-05000BB-SPCL: 5000 Torr) measured the gas pressure in the thermal chamber.

2.1.4 Solar Simulator Arc-Lamp and Elliptical Collector Mirror

A solar simulator argon arc-lamp (Vortek Industry Ltd., Model 110-150) used for the optical heating of the thermal chamber containing the gas propellant. The lamp could be produced a maximum of 60 kW optical radiation (with a maximum 150 kW$_e$ power input) and operated continuously in high pressure argon gas. The arc was deionized water cooled, operated in DC, and vortex-stabilized within a single quartz tube. Rapidly swirling water on the inner surface of the lamp tube efficiently removed excess heat and prevented deposition of the electrode material. Assemblies at each end of the lamp house user-replaceable water-cooled tungsten electrodes. The diameter and length of the lamp were 11 mm and 165 mm, respectively. Deionized water and argon gas were circulated, filtered, and cooled by the cooling/gas system. A pump recirculated deionized water through a water-heat exchanger in a closed loop system for cooling the arc lamp.

The water-cooled elliptical trough mirror had a length of 152 mm and the major and minor radii of 125 mm and 75 mm, respectively. The inside surface of the trough mirror was coated with rhodium of 1.0×10^{-6}-inch (minimum thickness) on the nickel coated under-plate of 0.0002" (minimum thickness). The reflectivity was measured to be

5

about 60% for 632.7-nm light of He-Ne laser. The elliptical trough mirror reflected the light emitted from the arc-lamp and line-focus it on the surface of the thermal chamber.

2.1.5 MPD Thruster

The MPD thruster, shown in Figure 3, consisted of a hollow cathode and flared anodes which were known to be superior to the conventional ones as mentioned in Ref. 5. It was operated in study-state self-field mode with 2 welding power supplies (Miller Electric Mfg. Co., Gold Star 600 SS) in series which provided up to 1200 A at 44 V DC at 60% duty cycle. The power could be delivered by two different anodes, as seen in Fig. 3, which lowered the voltage and current of each anode and consequently reduced anode fall voltage that causes low efficiency [13]. The half angle of the thoriated tungsten nozzle in some experiments was 25^0 in which the efficiency of MPD thruster was considered. The diameters of the tips of the stainless steel hollow cathode and water-cooled anode were 37 mm and 60 mm, respectively, and the thickness of the machinable glass ceramic (macor) insulator was 16 mm. The stainless steel ring between the insulator and thoriated
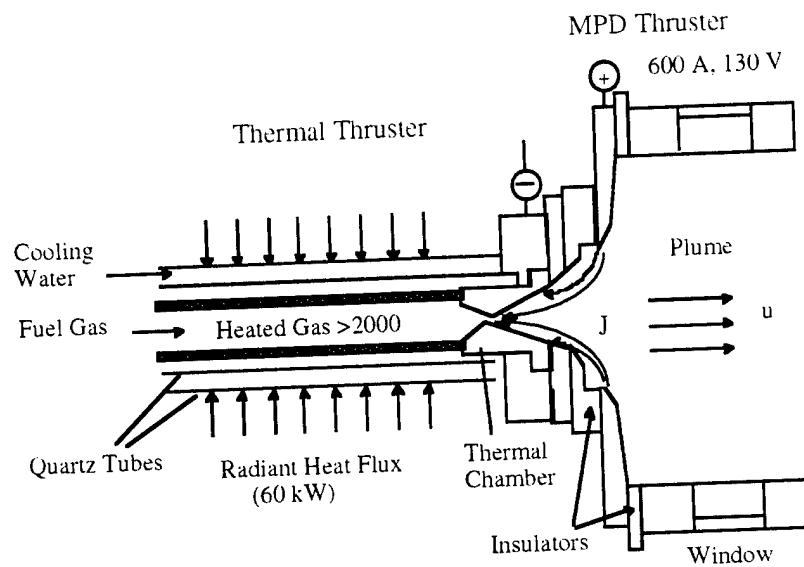

Figure 3. Cross section of the STEP system

tungsten nozzle was needed to hold the thermal chamber with enough strength. The rear side of the anode expanded very fast to the test section, which was connected to a large vacuum tank that simulated the space environment very soon after the thruster.

Figure 4 shows a modified MPD thruster diagram. The half angle of the copper-tungsten tip nozzle is 7.5^0. For chemical thruster without the MPD acceleration, optimum divergence cone half-angles are generally 12^0 - 18^0 [9, 14]. The diameter of the

6

hollow cathode tip was 12 mm, the thickness of the ceramic insulator was 12.7 mm, the thickness and the inner diameter of the water-cooled brass anode disk were 19.09 mm and 20.2 mm, respectively.

The hollow cathode of the MPD thruster also acts as the nozzle of the thermal thruster from which a thermal plume is ejected into the MPD chamber.
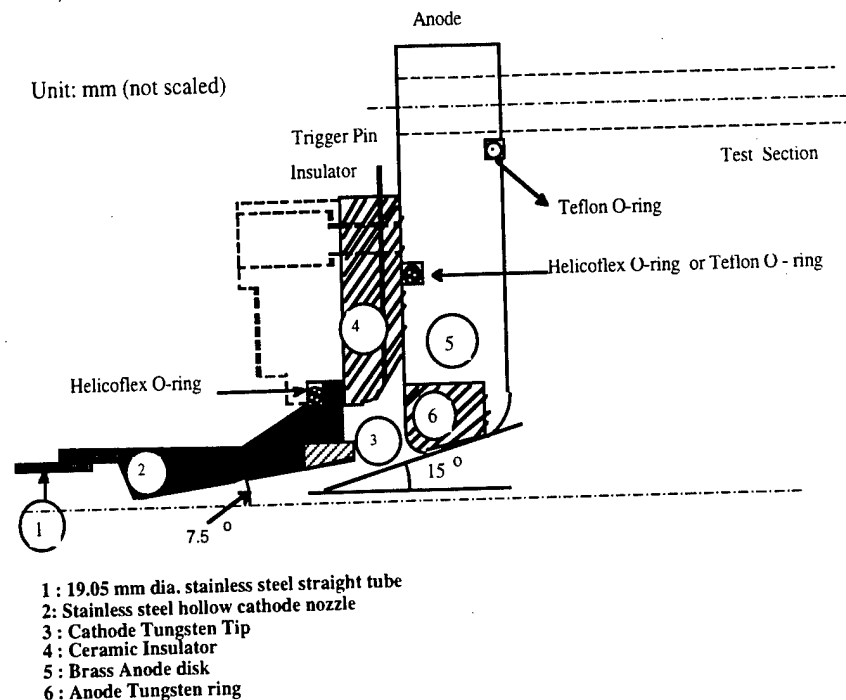

1 : 19.05 mm dia. stainless steel straight tube
2: Stainless steel hollow cathode nozzle
3 : Cathode Tungsten Tip
4 : Ceramic Insulator
5 : Brass Anode disk
6 : Anode Tungsten ring

Figure 4. Diagram of a modified MPD thruster

2.1.6 Test Section and Diagnostic Instruments

The two test sections were placed between the MPD thruster and the gate valve of the vacuum tank. The first section has 3 windows of 2.5" diameter each and the second section has 4 windows of 5" diameter each to allow access of the diagnostic tools for measuring the physical parameters of the exhaust propellant such as velocity, density, and temperature. The interface of the first section is met with the MPD nozzle and the 8" second test section. The larger diameter of the windows of the second section provides access of the laser beam to measure the propellant velocity at the nozzle exit.

A mass flow meter (Teledyne Hasting Instruments, 203/400, calibrated for the range of 0-300 SLPM argon) measures the total mass flow rates of the system. A simple Pitot tube was made of stainless steel with 2.5-mm inner diameter and 3.175-mm of outer diameter and used to measure the local total pressure of the propellant. Its front end was

7

smoothly shaped and reduced the inner diameter down to 2.0-mm to receive the impact local total pressure. It then located at a distance of 77 mm (just after the MPD thruster) from the nozzle throat and connect with a pressure transducer and readout (MKS Model # 122AA, 0-100 Torr, 0-10 VDC analog signal and MKS PDR-D power supply & readout). Figure 5 shows the arrangement of the Pitot tube for total pressure measurements.

The temperatures of the nozzle throat and electrodes were also measured by a thermal imaging system (Inframetric Corp., Model 600L: wavelength range = 8-12 μm, Scanning rate = 8000 Hz in horizontal, 60 Hz in vertical.

A pressure transducer (MKS Instrument Co., MKS Model 122BA-00001AB: 1 mTorr) measures the pressure of the test section.

A data acquisition system (NI Co., LabVIEW) gathers the data from an oscilloscope (Tektronix Inc., TDS 520): digital 500 MS/s), the pressure transducers, and thermocouples.
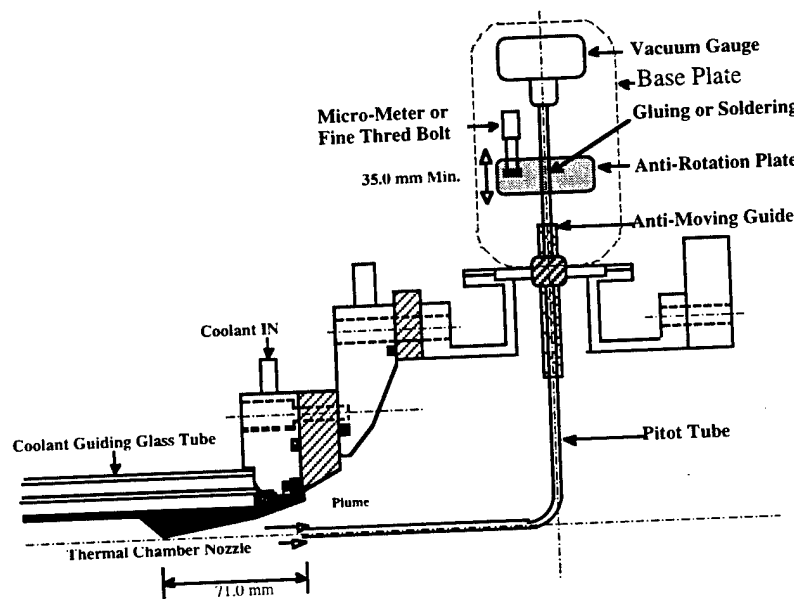

Figure 5. Pitot tube arrangement for total pressure measurements

A pulsed dye laser (Lambda Physik, LPD 3002CES: Tuning range 332 nm - 860 nm) pumped by an excimer laser (Lambda Physik, LPX 220I CC: Computer controlled, maximum average power of 120 mJ, pulse duration of 12 ns) has been installed for the non-intrusive diagnosis by the laser-induced fluorescence (LIF) method [Ref. Keffer]. An output power of 11 mJ per pulse was obtained from the laser when Rodamine 6G was used for the dye to emit a laser beam of 570 nm. A spectrometer (Thermo Jarrell Ash Corp., Jarrell Ash Monospec 27 Model 82-499: focal length=275 mm) and OMA

(Thermo Jarrel Ash Corp., LAMDA LS-200: 2048 pixels, 14 μm/pixel) system and lock-in amplifiers are to be used for the analysis of the fluorescence light. Figure 6 shows the schematic diagram of the LIF method.
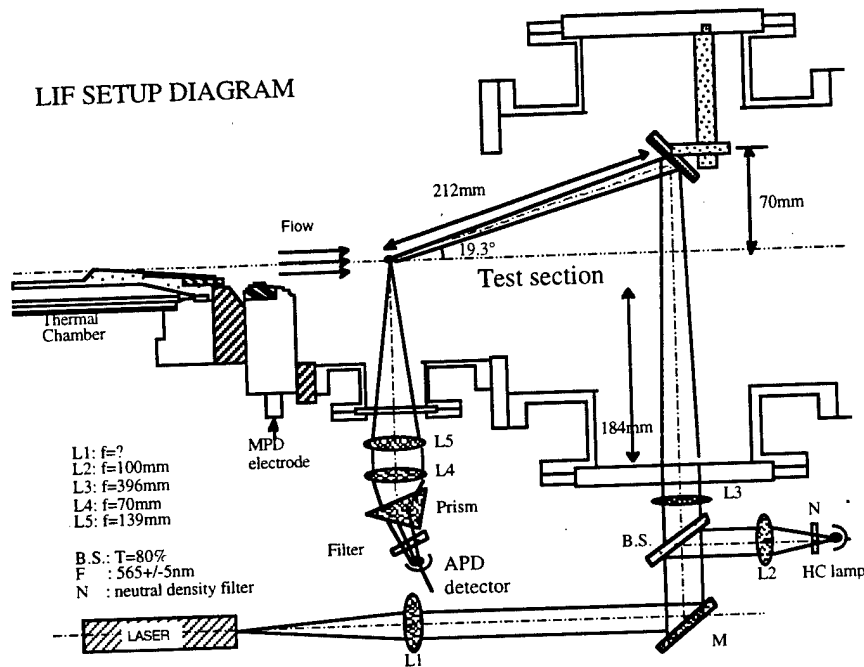

Figure 6. Schematic diagram of the LIF technique

2.1.7 Vacuum Facilities

A large vacuum tank (Modern Welding Company: volume = 30 m^3), a gate vale with electropnuematic actuator (GNB Corp., G12PSO: 12 inches) and a 3-stage mechanical vacuum pump system (Kinney Vacuum Co., Model KMBD-4501/KMBD-400/KD-50 Mechanical Booster System: Pumping speed = 84 m^3 min at 1 Torr with 2700 rpm) are setup to make the environment of space after the MPD thruster. The leak rate of the vacuum tank was measured to less than 11 mTorr in 8 hours at initial pressure of 1 mTorr.

2.2 Experimental Results and Accomplishment

During the grant period, the following measurements were accomplished and their results were presented in AIAA annual professional meetings.

2.2.1 The system pressure differential

The measured system pressure differential across the nozzle throat as well as the measured static and total pressures (on the window and on the center line, respectively)

9

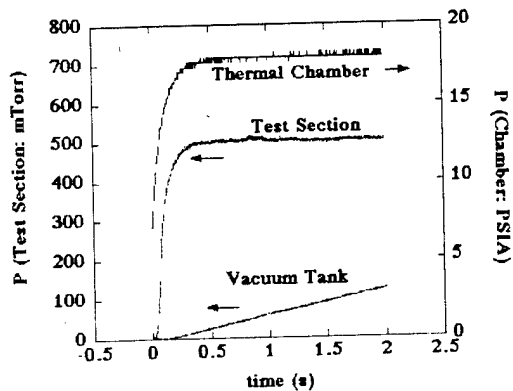were shown to be adequate as were expected. The results of these measurements are shown in Figures 7 a and 7 b.
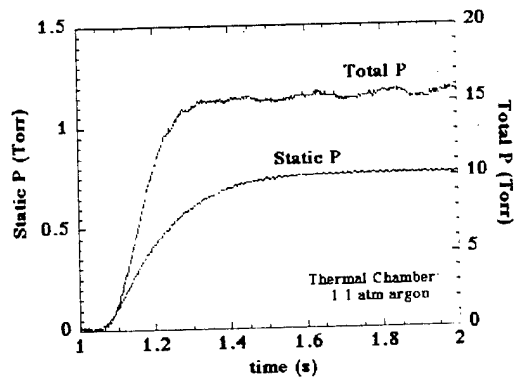

Figure 7 a. System pressure differential.

Figure 7 b. Variation of the total pressure on the center line and the static pressure on the window.

2.2.2 Optical heating of thermal chamber

As mentioned in the above, a solar simulator arc-lamp is used for the heating of thermal chamber in turn the propellant inside it. In order to examine the solar simulator before proceeding heating and propulsion experiments, a stainless steel thermal chamber having an outer diameter of 19 mm, was employed inside the elliptical mirror. Two K-type thermocouple were placed inside the thermal chamber to measure the temperature at the throat and at the wall. Temperature-rises of the throat are plotted in Figure 8 for different brightness of the arc-lamp which was proportional to the electric power flowing through the lamp. The temperature rose faster as the electric power was increased from 6.5 kW to 24.5 kW. The temperature increments from room temperature were linear to the at 90 second after turning on the lamp as seen in Table 1. For the electric power input of 6.5 kW the temperature was measured to be leveled at 800 K in 12 minute after turning on the lamp.

The temperature-rises at the center and throat of the thermal chamber are compared as shown in Figure 9 (a) and (b) which were measured with the arc-lamp current of 50 A. The center was heated faster than the throat that was closer to a holder in which cooling water flowed. Plot (c) and (d) on the Figure 9 are the corresponding theoretical results at the center and throat that were calculated by the time-dependent 1-D heat transfer equation [15]as follows

Table. 1. Temperature increments vs the optical power
emitted from the lamp 90 s after turning on the lamp.
The temperature increments are proportional to the power.

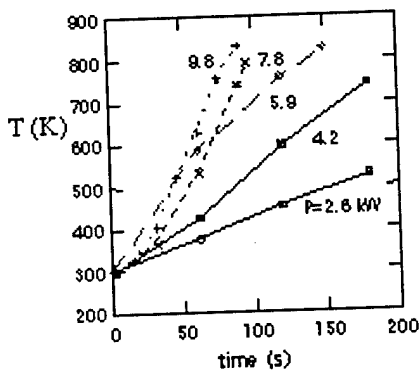| Optical Power (kW)	Temperature Increment (K)
2.6	115
4.2	220
5.9	370
7.8	443
9.8	533

Fig. 8. Temperature rises in time at the throat of
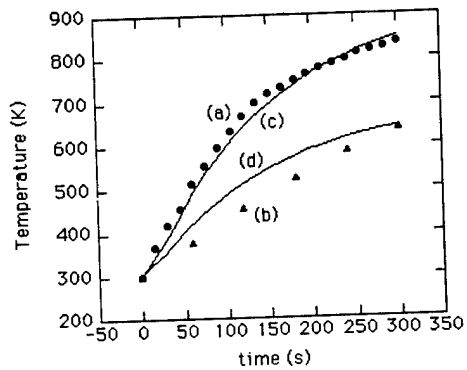steel thermal chamber for different
optical powers.

Fig. 9. Plots of Temperature-rises (a) at the
center, (b)throat and the corresponding
theoretical calculation at (c) the center
and (d) throat.

$$c_p \rho_l \frac{dT_s}{dt} = k \frac{dT_s}{dz} + q_{irr} - \sigma T_s^4 .$$

The specific heat c_p of iron is 478 J/(kg-K) at 100 ^{0}C and 665 J/(kg-K) at 500 ^{0}C
[16]. The heat conductivity k of steels 6.83x10^5 J/(m^3-s-K) at 100 ^{0}C and 2.19x10^5 J/(m^3-s-K) at 800 ^{0}C [The same Ref.] The line density ρ_l is 0.984 kg/m that is estimated from
the multiplication of the density ρ of 7874 kg/m^3 by the cross-sectional area A of
1.25x10^{-4} m^2. The radiant flux q_{irr} per unit length was estimated to be 1404 J/(s-m) from
the following relation:

$$q_{irr} = \varepsilon_{chamber} t_{quartz} r_{mirror} \kappa_{light} P_{electric} / l,$$

where the absorptivity of the stainless steel chamber $\varepsilon_{chamber}$ was set as 0.45 at 500 nm, the transmitance of the two quartz tubes t_{quartz} as 0.9, the coupling constant of the elliptical mirror reflectivity r_{mirror} as about 0.2, the conversion factor of the electric power to the light κ_{light} as 0.4 given by the Vortek [Manual 19], and electric power of the solar simulator $P_{electric}$ as 6.5 kW. The length of the irradiated part of the thermal chamber l was 150 mm.

Figure 10 shows the spectrum of the arc-lamp irradiance measured on the surface of the thermal chamber in the range of 380 - 940 nm in order to calculate the optical power coupled into the thermal chamber. The 27-cm spectrometer with the gratings of 150, 600, and 1200 gr/mm was used to analyze the light through an fused silica UV-fiber optics. The detailed description of the measurements appears in Ref [18]. The continuum is intense in the range of 380 - 600 nm and a plenty of line emissions of argon in the IR region. The color temperature estimated from the continuum to be 6000 K.
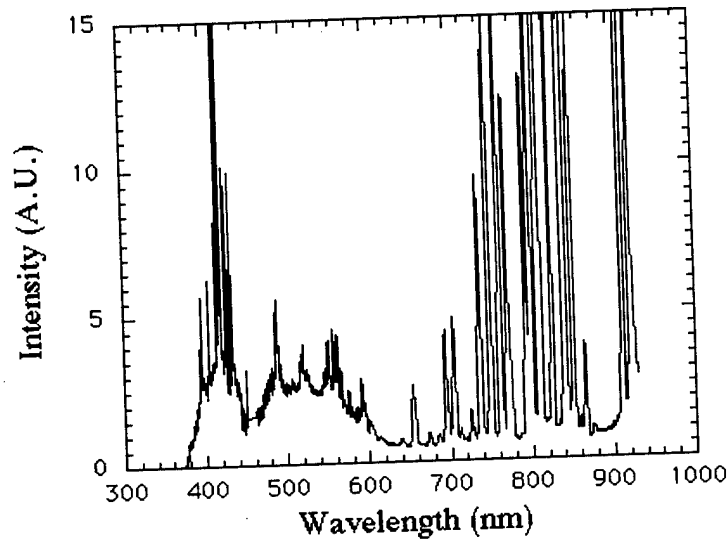

Figure 11. Spectrum of the solar simulator arc-lamp irradiance

2.2.3 Effect of heat on total pressure

The thermal plume has been characterized and benchmarked for the next step with MPD acceleration. Argon gas was used as propellant for thermal plume study. The radial profiles of the total pressure were measured with the Pitot tube at the two different locations from a 2.0-mm diameter nozzle throat. The results of these measurements are shown in Figures 11 and 12 at the distance of 99 mm and 71 mm from the nozzle throat, respectively, and at room temperature and 813 K. The chamber pressure was kept

12

constant at 203.0 kPa and mass flow rates were 49 SLPM at room temperature and 41 SLPM at 873 K, respectively. The measured radial total pressure at the distance of 99 mm showed that the profile is parabolic and symmetrical but changes its shape and amplitude with the increase of temperature (see Fig. 11).
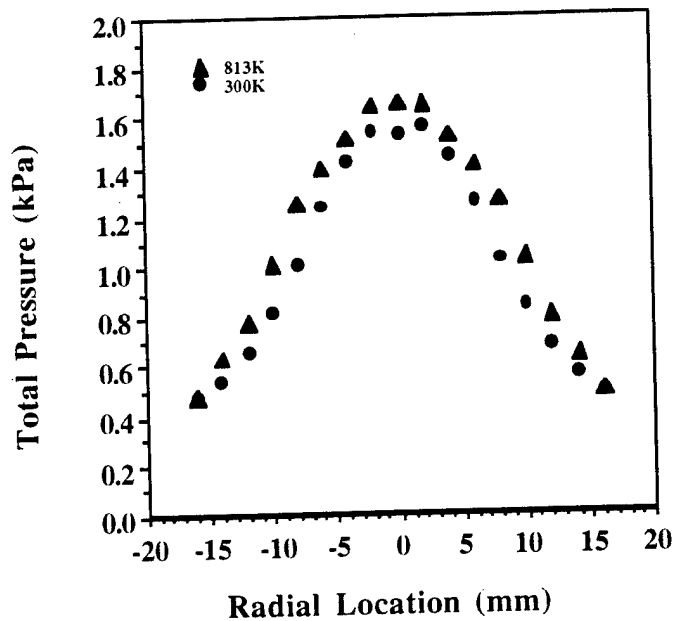
Figure 11. Total pressure radial profile with argon at 99 mm from the nozzle throat.

The radial profiles of total pressure obtained at the distance of 71 mm from the nozzle throat showed an agreeable distribution with those given by CET93. At higher thermal chamber temperature, the nozzle flow has a peaked total pressure as shown in Fig.12 indicating a peaked velocity distribution at the edge of the flow. The total pressure measured with the Pitot tube is in fact the measure of the thrust density.
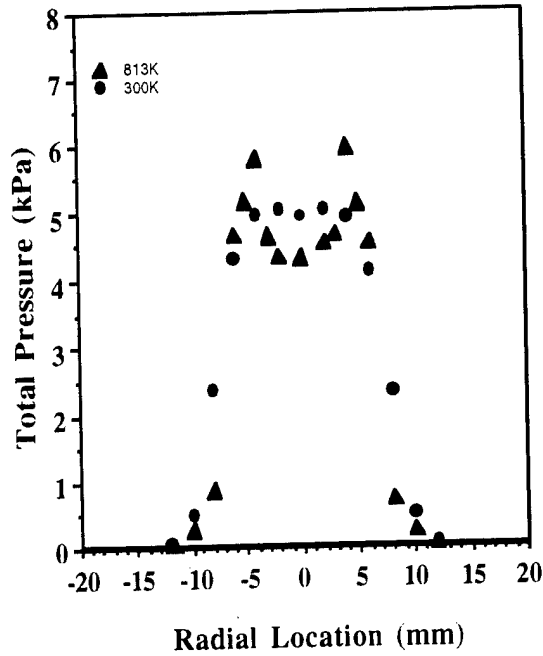
Figure 12. Total pressure radial profile with argon
at 71 mm from the nozzle throat.

These data were used to calculate the specific impulse and thrust density for the thermal thruster. The resulting specific impulse and thrust density are then compared with those given by CET93 program as shown in Fig. 13 & 14, respectively. A more than 80% increase in I_{sp} obtained by heating is about 20% larger than that of the CET93 program. The mass flow rate however, is lower than that given by CET93 program for 2 mm diameter nozzle throat.
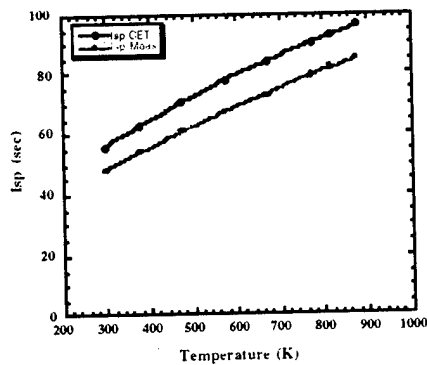

Fig. 13. Comparison of I_{sp} obtained from the measured data to that of calculated from CET93 code.
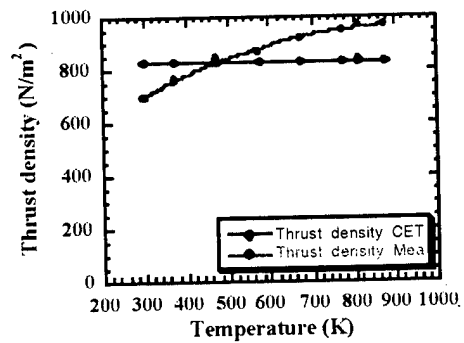

Fig. 14. Comparison of the thrust obtained from the measured data and that of calculated from CET93 code.

14

2.2.4 Effect of MPD on total pressure

A preliminary test run with the application of the MPD has been made. The MPD thruster was a steady-state self-field thruster that used 2 DC power supplies in series, which could provide DC currents up to 600 A at 30 V with an open-circuit voltage of 130 V. Figure 4 shows the modified MPD thruster diagram. The half angle of the thoriated tungsten tip nozzle is 7.5^0. The diameter of the hollow cathode tip is 12 mm, the thickness of the ceramic insulator is 12.7 mm, the thickness and the inner diameter of the water-cooled brass anode disk are 19.05 mm and 20.2 mm, receptively. The total pressure of the flow was measured with the Pitot tube at the exhaust plane of the MPD accelerator. The thermal chamber pressure was kept constant at 203.0 kPa and the gas temperature was at ~300 K. The open-circuit voltage of the MPD power supply was 130 V.

Figure 15 shows the total pressure measured by the Pitot tube on the axis of the flow and with MPD currents ranging from 0 A to 500 A. The total pressure 3.36 kPa measured for the room temperature (~300 K) and running without the MPD on was noted as benchmark to measure any effect of the applied MPD. This initial test with MPD showed that the total pressure of argon propellant did not change appreciably at the currents lower than 150 A (at 23.0 V). At the currents of 200 A (at 17.0 V) and higher, the total pressure was increased significantly. A total pressure of 4.72 kPa was measured with the current of 500 A (40% increase from 3.36 kPa) which indicates in turn the increase of the thrust and specific impulse of the system. This result is expected from the simple relation

$$P_{total} = P_{static} + \frac{1}{2}\rho V^2$$

and the combined thermal and MPD thrust statement

$$T_{total} = \dot{m}(V_{thermal} + \Delta V_{MPD})$$

Where, T_{total} is the total thrust.

From the relative increase in total pressure, thus the thrust is approximately increased by 40%. Since $\Delta T_{total} \sim \Delta P \sim I^2$, a large increase in thrust is expected for the full current of 600 A in near future.
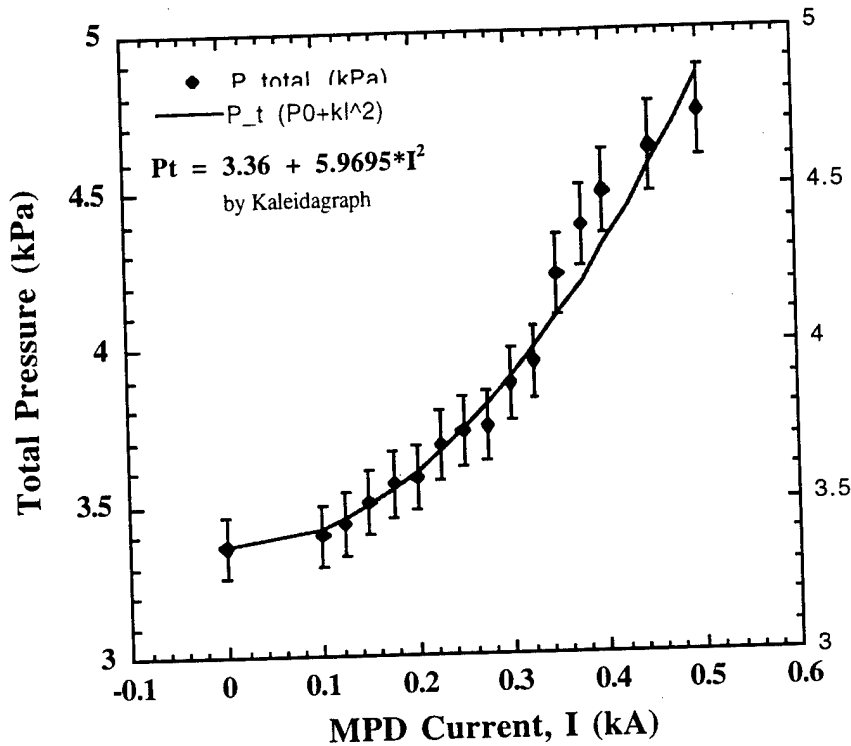
MPD Current Dependence of Total Pressure

Figure   .MPD current dependence of total pressure

2.2.5 Summary

A solar thermal-electric propulsion (STEP) system has been installed to develop a rocket engine having medium ranges of specific impulse and thrust. The STEP system was consisted of a solar thermal and a magnetoplasmadynamic (MPD) thrusters in a tandem arrangement. The spectral irradiance of the solar simulator arc-lamp was measured in order to determine the optical power coupled into the thermal chamber. The spectrum of the arc-lamp light had both continuum of a blackbody radiation whose peak was around 500 nm and intense line radiation of argon. The temperature of the thermal chamber rose faster with the increase of the power of the arc-lamp as was expected from the calculation.

As a proof-of-concept of the STEP system, the plume that is exhausting from the thermal chamber had been characterized and benchmarked for the next step with the MPD acceleration. The total pressures of the plume measured at different location and temperature showed that the radial profiles are symmetrical but change its shape and amplitude with the increase of temperature as expected. However, the results are slightly excessive than that of one dimensional-code prediction. This discrepancy may be caused

by the use of a Pitot tube in a supersonic flow. Nevertheless its use for a relative measurement to recognize the qualitative of the MPD acceleration is justified.

A preliminary test run with the application of the MPD has been made. The relative increase of the total pressure, therefore the thrust, was approximately 40% when 500 A current applied on the MPD electrodes. With the encouraging results from the MPD preliminary test, we are pursuing quantitative determination of the effect of the MPD acceleration on the thrust and the specific impulse of the system by using a laser-induced fluorescence technique to measure the absolute velocity of the exhausted plume.

3. References

[1]   M.A. Birkan and M.M. Micci; "Survey of Electric Propulsion Thruster Applicability to Neär Earth Space Missions"; Proceedings of DGLR/AIAA/JSASS 20th International Electric Propulsion Conference, 374-382 Garmisch-Partenkirchen, (1988).

[2]   M.A. Birkan; "Laser Propulsion: Research Status and Needs"; J. of Propulsion and Power 8 (2), 354-360 (1992).

[3]   R.M. Myers; "Electromagnetic Propulsion for Spacecraft"; AIAA-93-1086; AIAA/AHS/ASEE Aerospace Design Conference, February 1993.

[4]   M.T. Domonkos, A. Gallimore, R.M. Myers, and E. Thompson; "Preliminary Pulsed MPD Thruster Performance"; AIAA-95-2674; 31st AIAA/ASME/SAE/ASEE Joint Propulsion Conference and Exhibit, San Diego, CA, July 1995.

[5]   H.L. Kurtz, M. Auweter-Kurtz, W. Merke, and O. Schrad; "Experimental MPD Thruster Investigations"; AIAA-87-1019; 19th International Electric Propulsion Conference, Colorado Springs, CO, May 1987.

[6]   M.A. Mantenieks and R.M. Myers; "100 kW Class Applied MPD Thruster Component Wear"; 10th Symposium on Space Nuclear Power and Propulsion, AIP Proceedings No. 271, 1317-1326 (January 1993).

[7]   F. Paganucci and M. Adrenucci, "MPD thruster performance using pure gases and mixtures as propellant", AIAA-95-2675, 31th AIAA/ASME/SAE/ASEE Joint Propulsion Conference, San Diego, CA, July 1995.

[8]   J. P. Schleiniz and R. E. Lo, "Solat-thermal OTVS in comparison with electrical and chemical propulsion systems", 38th Congress of the international astronautical   federation, Bridhton, UK, October 1987.

[9] G. P. Sutton, "Rocket Propulsion Elements", 5th Ed., John Wiley and Sons Inc., New York, 1986, Chapter 1.

[10] B.M. Tabibi, S.H. Choi, and J.H. Lee; "Thermal-Electric Propulsion with Magnetoplasmadynamics Acceleration"; AAIA-94-2468; 25th AIAA Plasmadynamics and Lasers Conference, Colorado Springs, CO, June 1994.

[11] S.H. Choi, J.H. Lee, and B.M. Tabibi; "Solar Thermal-Electric Propulsion For Upper-Stage Applications"; AIAA-95-2574; 31st AIAA/ASME/SAE/ASEE Joint Propulsion Conference and Exhibit, San Diego, CA, July 1995.

[12] Y. S. Choi, D. X. Nguyen, B. M. Tabibi, and J. H. Lee, "Installation and Preliminary Operation of a Solar Thermal-Electric Propulsion System", AIAA 96-2321, 27th AIAA Plasmadynamics and Lasers Conference, June 17-20, 1996.

[13]. A. D. Gallimore, A. J. Kelly, and R. G. Jahn, "Anode Power Deposition in Quasi-steady Magnetoplasmadynamic Thrusters", J. of Propulsion and Power **8** (6), 1224-1231 (1992).

[14] G. V. R. Rao, "Recent Developments in Rocket Nozzle Configurations", ARS J. **31** (11), 1488, (1961).

[15]. J. W. Cornelisse, "Rocket Propulsion and Spaceflight Dynamics", Fearon-Pitman Publishers Inc., London, Belmont,CA. 1979.

[16] W. H. Kohl, "Handbook of Materials and Techniques for Vacuum Devices", Reinhold Publishing Corporation. New York, 1994.

[18] B.M. Tabibi, C.A. Terrell, J.H. Lee, and G. Miner; "CW iodine laser performance of t-C_4F_9I under closely-simulated air -mass-zero solar pumping"; Optics Communications **109**, 86 (1994).

4. Publications and Presentations

1. B.M. Tabibi, S.H. Choi, and J.H. Lee; "Thermal-Electric Propulsion with Magnetoplasmadynamics Acceleration"; AAIA-94-2468; 25th AIAA Plasmadynamics and Lasers Conference, Colorado Springs, CO, June 1994.

2. S.H. Choi, J.H. Lee, and B.M. Tabibi; "Solar Thermal-Electric Propulsion For Upper-Stage Applications"; AIAA-95-2574; 31st AIAA/ASME/SAE/ASEE oint Propulsion Conference and Exhibit, San Diego, CA, July 1995.

3. Y. S. Choi, D. X. Nguyen, B. M. Tabibi, and J. H. Lee, "Installation and Preliminary Operation of a Solar Thermal-Electric Propulsion System", AIAA 96-2321, 27th AIAA Plasmadynamics and Lasers Conference, June 17-20, 1996.

4. Dung X. Nguyen, Cecily J. Smith, Bagher M, Tabibi, and Ja H. Lee, "Preliminary Operation of a Solar Thermal-Electric Propulsion (STEP) System", Bulletin of the APS, Program of the 1996 Fall Meeting of the SESAP Society, Vol. 41, No, 8, November 1996. Abstract AB 5.

6. Dung X. Nguyen, Matthew K. Nam, Bagher M. Tabibi, and Ja H. Lee, "Performance of Thermal Plume in Solar Thermal-Electric Propulsion System", 33rd AIAA/ASME/SAE/ASEE Joint Propulsion Confrence & EXHIBIT, July 6 - 9, 1997 / Seattle, WA. paper AIAA 97-3207.

7. Bagher M. Tabibi, et. al.," Non-Intrusive Optical Diagnostic Methods for Flowfield Characterization", Proceeding of the NASA URC Technical Conference, Vol. 1, pp. 711-716, 1997.

8. Darrell A. Spraggins, Bagher M. Tabibi, Ja H. Lee, and Leonard M. Weinstein, "A Small-Field, High-Sensitivity Focusing Schlieren System for Flowfield Visualization", Bulletin of the APS, Program of the 1996 Fall Meeting of the SESAP Society, Vol. 41, No. 8, November 1996. Abstract AC 9.

9. D. X. Nguyen, M. Thaik, Y. S. Choi, C. A. Terrell, B. M. Tabibi, and J. H. Lee, "Thermal-Electric Propulsion with Magnetoplasmadynamic Acceleration," Bulletin of the APS, Vol. 40, No. 13, Nov. 1995.

5. Student Training on STEP Project

Doctoral Candidate					
Name	Citizen	Gender	Major	Date of Employ.	Expected Date
1. Nguyen, Dung X.	US	Male	Physics	1994	1998

M.S. Degree Candidate					
Name	Citizen	Gender	Major	Date of Employ	Expected Date
1. Thaik, Myo	Berma	Male	Physics	1994	Transfered to RCOP in 1995

Undergraduate Student					
Name	Citizen	Gender	Major	Date of Employ	Expected Date
1. Goss, Tyhesha	US	Female	Physics	1995	1995
2. Fields, Aisha	US	Female	Physics	1996	1996
3. Barlow, La Venta	US	Female	Engineer	Summer 1995	
4. Creekmore, Santiel	US	Male	Physics	Summer 1996 & 1997	

6. Scientific Personnel Participated in STEP Project

	Name	Citizenship	Employment Period
1.	Tabibi, Bagher M., Ph. D. PI	US	1994 - 1997
2.	Lee, Ja H., Ph. D. Faculty Associate	US	1994 - 1997
3.	Choi, Sang H., Ph. D. Consultant	US	1994
4.	Choi, Yoon S., Ph. D. Postdoctoral	Korean	1994 - 1996
5.	Nam, Matthew K., Ph. D. Postdoctoral	US	1997